Creep-Fatigue Properties of Additional 316H PM-HIP Materials Fabricated from Different Powder Compositions and Processing Routes

INL/RPT-24-75644
Revision 0

Microreactor Program

SEPTEMBER 2024

Tate Patterson,

Idaho National Laboratory

Yanli Wang

Oak Ridge National Laboratory

Idaho National Laboratory

Battelle Energy Alliance manages INL for the U.S. Department of Energy's Office of Nuclear Energy

INL/RPT-24-75644
Revision 0

Creep-Fatigue Properties of Additional 316H PM-HIP Materials Fabricated from Different Powder Compositions and Processing Routes

Tate Patterson,
Idaho National Laboratory
Yanli Wang
Oak Ridge National Laboratory

September 2024

Idaho National Laboratory
Microreactor Program
Idaho Falls, Idaho 83415

https://gain.inl.gov/SitePages/MicroreactorProgram.aspx

Prepared for the
U.S. Department of Energy
Office of Nuclear Energy
Under DOE Idaho Operations Office
Contract DE-AC07-05ID14517

Page intentionally left blank

ABSTRACT

The process of powder metallurgy (PM) hot isostatic pressing (HIP) works by consolidating powdered materials at relatively high temperature and pressure to form near-net-shaped components. Ideally, PM-HIP production methods can reduce component lead time and improve designs for high-temperature reactors and/or microreactors. To introduce PM-HIP into Section III, Division 5 of the American Society of Mechanical Engineers Boiler and Pressure Vessel Code, it is necessary to show adequate material properties regarding creep, high-temperature low-cycle fatigue, and creep fatigue. However, prior work has shown that the creep-fatigue cycles to failure for PM-HIP 316H stainless steel are greatly reduced compared to the conventional, wrought product. This work continued creep-fatigue analysis on a 316H stainless steel with lower oxygen and nitrogen contents and at different HIP parameters than previously analyzed. The objective was to better understand what is causing the reduced PM-HIP 316H performance so improvements can be made PM-HIP 316H creep-fatigue lifetimes.

ACKNOWLEDGEMENTS

This work was sponsored by the United States Department of Energy (DOE) under Contract No. DE-AC07-05ID14517 with Idaho National Laboratory (INL), which is managed by Battelle Energy Alliance, and under Contract No. DE-AC05-00OR22725 with Oak Ridge National Laboratory (ORNL), which is managed and operated by the University of Tennessee– Battelle LLC. Programmatic direction was provided by the Microreactor Program of the Office of Nuclear Reactor Deployment of the Office of Nuclear Energy (NE).

The authors gratefully acknowledge the support provided by Diana Li of DOE-NE, Microreactor Program (MRP) federal manager. Additionally, the authors thank John Jackson of INL and MRP national technical director, and Holly Trellue of the Los Alamos National Laboratory and the technology maturation technical area lead. The authors also thank Richard Wright of Structural Metals, LLC, and Ryan Rupp and Ting-Leung (Sam) Sham of the United States Nuclear Regulatory Commission for their helpful discussions, reviews, and support. The authors also acknowledge Joel Simpson of INL for performing low-cycle-fatigue and creep-fatigue testing and Michael Mulholland of INL for performing additional heat treatments.

CONTENTS

FIGURES

TABLES

ACRONYMS

ASME	American Society of Mechanical Engineers
ASTM	American Society for Testing and Materials
BPVC	Boiler and Pressure Vessel Code
CF	Creep fatigue
DOE	Department of Energy
EBSD	Electron backscatter diffraction
EDS	Energy-dispersive spectroscopy
HIP	Hot isostatic pressing
INL	Idaho National Laboratory
IPF	Inverse pole figure
IQ	Image quality
LCF	Low cycle fatigue
MRP	Microreactor Program
NE	Office of Nuclear Energy
NRC	Nuclear Regulatory Commission
PM	Powder metallurgy

Page intentionally left blank

Creep-Fatigue Properties of Additional 316H PM-HIP Materials Fabricated from Different Powder Compositions and Processing Routes

1. INTRODUCTION

Powder metallurgy (PM) hot isostatic pressing (HIP) is a near-net-shape component fabrication process and considered an advanced-manufacturing production method. The PM-HIP process generally uses temperatures ranging from 0.7 to 0.9 times melting temperature to coalesce metallic powders, ranging from approximately 10 to 500 μm in powder particle diameter. The high temperatures accelerate diffusion while the isostatic pressure creates material consolidation through powder-to-powder contact to form fully dense sintered components. Benefits to the PM-HIP manufacturing process may include reductions in fabrication steps (i.e., by avoiding machining, welding, etc.) and potential for generating equiaxed grain structures.

For high-temperature nuclear reactor construction, the code endorsed by the Nuclear Regulatory Commission (NRC) is the American Society of Mechanical Engineers (ASME) Boiler and Pressure Vessel Code (BPVC) Section III "Rules for Construction of Nuclear Facility Components", Division 5 High Temperature Reactors [1]. Currently, Sec. III, Div. 5, does not include PM-HIP as a qualified manufacturing process. However, the ASME Sec. III, Div. 5, Task Group on AM Components considered PM-HIP to be a relatively mature technique for future incorporation into Sec. III, Div. 5. Additionally, wrought Type 316L, 316, and/or 316H—i.e., rolled or forged stainless steels—are qualified for use in ASME Section III, Division 5, for high-temperature, metallic pressure-boundary components. The idea of PM-HIP being a mature process, prime for introduction into high-temperature reactor applications, was based on the prior work that concluded that nitrogen up to 0.1 weight percent (wt%) and the lowest possible oxygen content is beneficial for mechanical properties [2-4]. A data package was compiled and resulted in Code Case N-834 [5] for PM-HIP 316L stainless steel for use in ASME Sec. III "Rules for Construction of Nuclear Facility Components", Div. 1 – Subsection NB Class 1 Components [6].

However, Rupp and Wright [7] initiated elevated-temperature creep-fatigue (CF) testing of PM-HIP 316 stainless steels and showed that there was a significant reduction in cycles to failure (approximately half) compared to conventional, wrought 316 stainless steel. Additional work expanded on the initial PM-HIP 316L analysis to include PM-HIP 316H stainless steel [8]. Each Type 316 stainless steels analyzed for CF performance has shown a considerable reduction in cycles to failure compared to wrought [1].

The objective of this work is to provide data for ASME BPVC Sec. III Div. 5 qualification and to understand the influences of chemical-composition and material-processing factors. This report contains mechanical-property and microstructure-characterization data on another 316H stainless steel powder that was procured and hot isostatically pressed by a commercial vendor.

2. EXPERIMENTAL METHODS

2.1. Materials

The composition of the commercially produced powder (tested before the HIP process) is shown in Table 1. Except for oxygen and nitrogen, all powder measurements were from the full powder fraction. However, oxygen and nitrogen were measured after sieving to 250 µm, which is most of the powder size distribution or full powder fraction. The compositions of the consolidated billets produced via two different HIP conditions are shown in Table 1. For reference, Table 1 also contains the composition requirements for ASME Sec. II, Part A [9] for 316H stainless steel plate (S31609); 316 stainless steel as defined in ASME BPVC Sec. III Div. 5 [1] for high-temperature use; and 316 composition reported in American Society of Testing of Materials (ASTM) A988/A988M-17, "Standard Specification for Hot Isostatically-Pressed Stainless Steel Flanges, Fittings, Valves, and Parts for High Temperature Service" [10]. The nominal sizes of Billet A and Billet B were 190 mm in diameter and 200 mm long, with the canned powders shown in Figure 1. The only differences between Billets A and B were the HIP parameters, which are shown in Figure 2.

Table 1. Measured powder and consolidated billet chemical compositions in wt%.

	316H Powder	PM-HIP 316H Billet A	PM-HIP 316H Billet B	SA 240 S31609 (316H)	ASME III Div. 5 (>595°C)	ASTM A988 S31600
Fe	Bal.	Bal	Bal.	Bal.	Bal.	Bal.
C	0.05	0.043	0.043	0.04–0.1	0.04–0.1	0.08
Ni	12.0	12.06	12.01	10.0–14.0	10.0–14.0	10.0–14.0
Cr	17.0	17.13	17.05	16.0–18.0	16.0–18.0	16.0–18.0
Mo	2.53	2.54	2.53	2.00–3.00	2.00–3.00	2.00–3.00
Cu	—	<0.01	<0.01	—	—	—
Ti	<0.003	<0.003	<0.003	—	≤0.04 *	—
Al	<0.01	0.003	0.005	—	≤0.03 *	—
Si	0.20	0.18	0.19	1.00	1.00	1.00
Mn	0.21	0.19	0.19	2.00	2.00	2.00
S	0.003	0.003	0.003	0.030	0.030	0.030
P	0.004	0.004	0.004	0.045	0.045	0.045
B	—	0.0003	0.0003	—	—	—
N	0.101	0.090	0.088	—	≥0.05*	≤0.10
O	0.012	0.0156	0.0149	—	—	—

NOTE: * Div.5 supplementary requirement for use at temperatures above 1,100°F (595°C).

Figure 1. Powder-filled cans prior to HIP (left) and final billets after can removal (right).

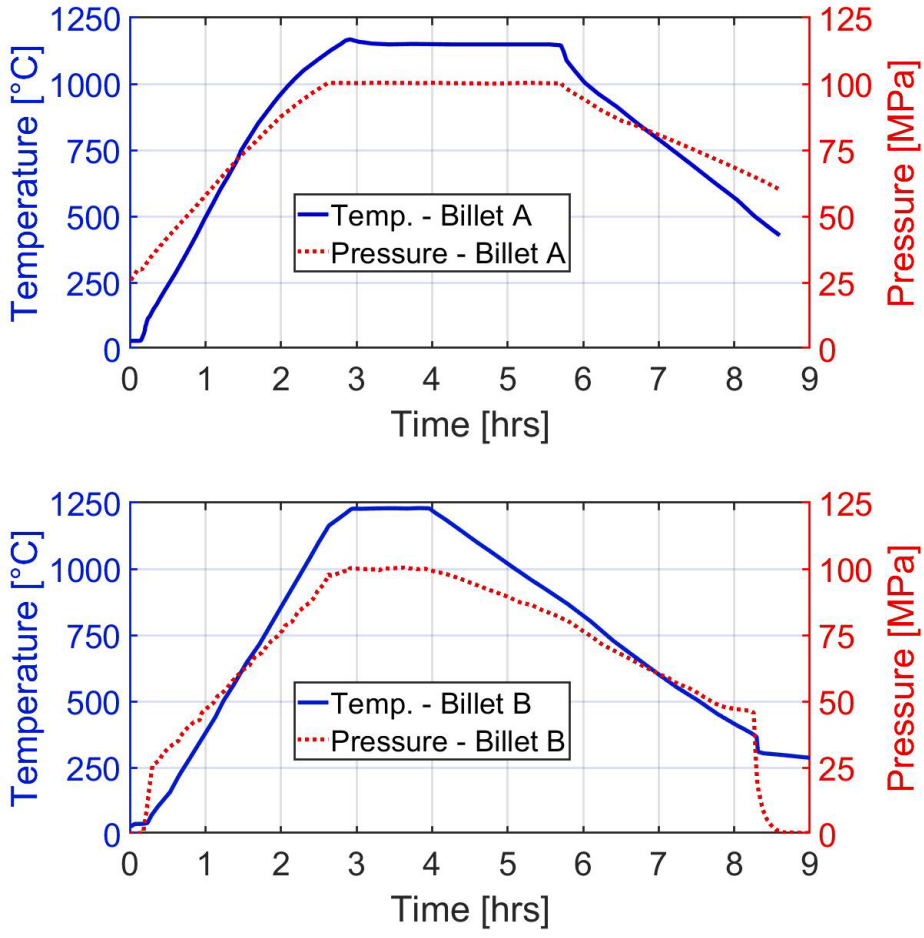

Figure 2. HIP parameters for Billet A (top) and B (bottom).

After HIP, the billets were exposed to a solution heat treatment at 1060°C for 4 hours, 10 minutes, followed by water quenching into a 16°C pool of water. The time from the furnace to quenching medium was approximately 35 seconds. The heat treatment was performed prior to removing the can (powder capsule) used for HIP. A photo of the billets positioned in the furnace is shown in Figure 3. The recorded furnace-zone temperatures and billet-temperature measurements are shown in Figure 4.

Figure 3. Photo of billets still in the cans in the solution heat-treatment furnace.

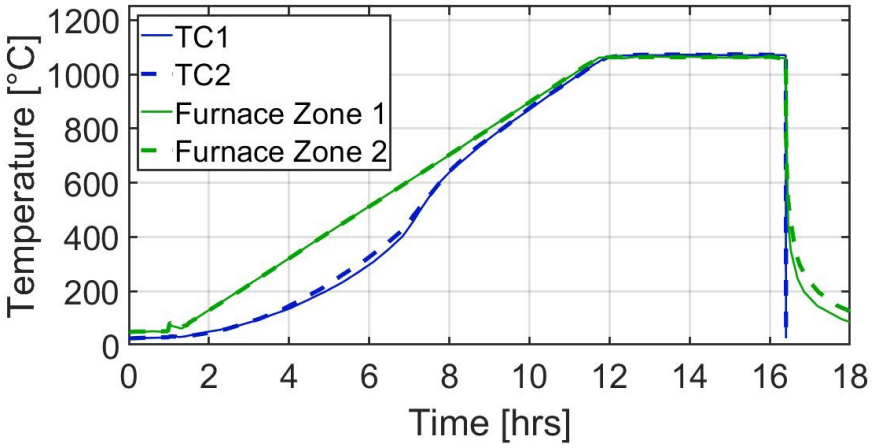

Figure 4. Solution heat-treatment thermal history showing furnace-zone temperatures and the temperatures of both billets.

An additional heat treatment was performed to determine the ability to grow grains after HIP. This heat treatment used a tube furnace, with the specimens exposed to atmosphere at 1200°C for 1 hour. The specimen sizes were approximately 10 mm × 10 mm × 50 mm. The furnace temperature was adjusted to match the reading from an R-type thermocouple inserted into the furnace and in contact with the specimens. The thermocouple measured temperature is shown in Figure 5.

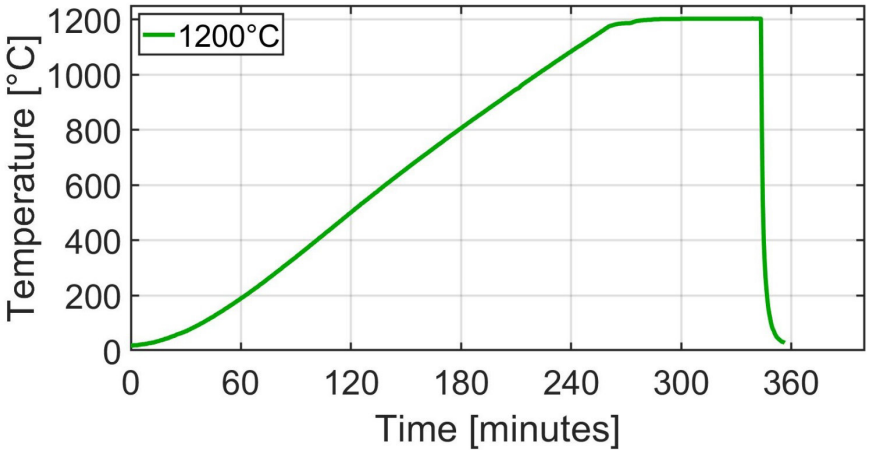

Figure 5. Additional heat treatment to determine the ability to grow the grains after HIP.

2.2. Microstructure Characterization

Metallographic specimens were sectioned and hot mounted in a thermosetting polymer, then ground with 400-, 600-, and 800-grit silicon carbide abrasive paper. Polishing steps used 6 and 3 μm polycrystalline diamond suspension and 0.05 μm colloid silica. For optical microscopy, electrochemical etching was performed using 10% oxalic acid at 3 V for approximately 20 seconds. Scanning electron microscopy was performed with the 316H stainless steel in the as-polished (unetched) state. For grain-size analysis, electron backscatter diffraction (EBSD) used an Ametek EDAX TSL camera, OIM Data Collection, and OIM Analysis software. Energy-dispersive spectroscopy (EDS) used an Octane Elect Plus C5 detector and EDAX TEAM software, Version 4.6.

2.3. Mechanical Testing

Table 2 shows the mechanical properties measured for each billet after the HIP and the solution heat-treatment process. The grain size, measured according to ASTM E112, "Standard Test Methods for Determining Average Grain Size," [11] were ASTM No. 8 (22.5 μm) and ASTM No. 7 (31.8 μm) for Billet A and Billet B, respectively. It should be noted that grain-size requirements for 316 stainless steels must be ASTM No. 7 or coarser for high-temperature applications, according to ASME BPVC Sec. III, Div. 5 [1]. Therefore, according to the optical measurements, Billet A would not meet wrought product requirements. However, Billet B is technically acceptable by meeting the finest grain-size threshold (ASTM No. 7). The trends in hardness and strength correlated with the grain-size measurements. Billet B had a slightly larger average grain size and showed decreased hardness and strength.

Table 2. Ambient-temperature mechanical properties as reported in the material test report for the for both billets of PM-HIP 316H stainless steel.

	PM-HIP 316H Billet A	PM-HIP 316H Billet B
Hardness [BHN 3000 kgf]	176	167
Yield Strength [MPa]	341	300
Tensile Strength at ≈20°C [MPa]	631	600
Elongation [%]	73	74
Reduction in Area [%]	52.5	54.5
Avg. Charpy V-Notch Energy at ≈20°C [J]	197±1.7	210±5
Grain Size [ASTM No.]	8	7

2.3.1. Elevated-Temperature Cyclic Testing

Elevated-temperature cyclic testing was based on E606/E606M-21, "Standard Test Method for Strain-Controlled Fatigue Testing" [12] and ASTM E2714-13, "Standard Method for Creep Fatigue Testing" [13]. However, the tests were conducted in accordance with INL's internal procedure, PLN-3346, "Creep Fatigue Testing" [14]. The fatigue and CF tests used servo-hydraulic load frames, three-zone furnaces, and strain control using a direct-contact extensometer. The temperature was controlled and monitored using two direct-contact R-type thermocouples. Both thermocouples were spot welded onto the opposing shoulders outside of each gauge section.

The low-cycle fatigue (LCF) tests were performed at 650°C using a full reversed strain (Δε) of ±0.5% and a strain rate of 0.001/s. Matching CF tests were performed with a tensile hold at peak strain for 30 minutes at the same temperature, strain range, and strain rate. Schematic examples of these testing procedures are shown in Figure 6. The number of cycles to failure was considered based on a 20% drop in the ratio of peak tensile stress to peak compressive stress (N_{f_20}). This approach was originally used by Totemeier and Tian [15] and is shown schematically in Figure 7. If the specimen ruptured in half prior to reaching the N_{f_20} failure criteria, the cycle just before failure was used as the number of cycles to failure.

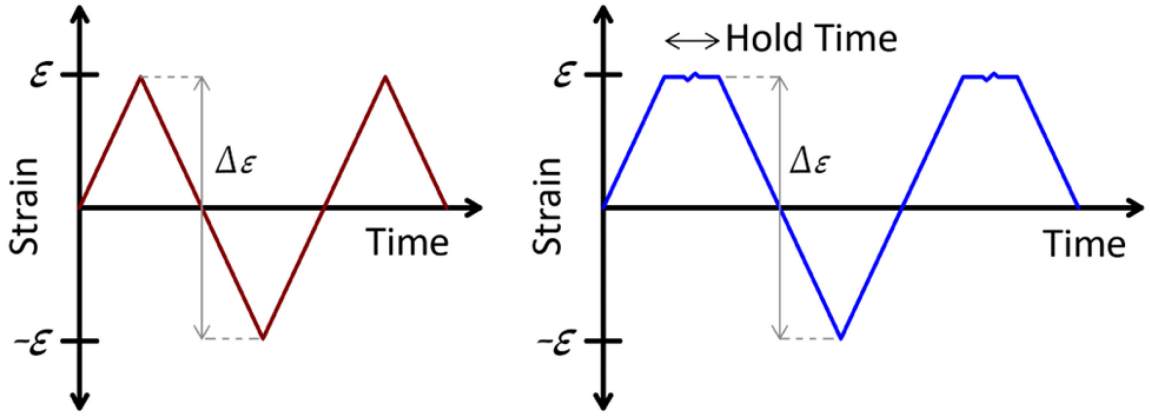

Figure 6. Schematics showing strain-controlled LCF (left) and creep-fatigue (CF, right) testing procedures.

$$r = \left| \frac{\sigma_{tensile}}{\sigma_{compression}} \right|$$

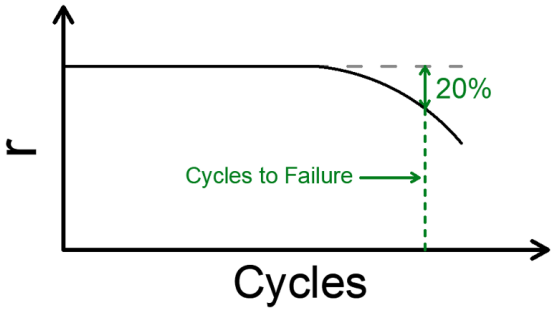

Figure 7. Evaluation criteria for cycles to failure based on a 20% stress reduction (N_{20}).

Another CF acceptance test was performed according to the wrought austenitic stainless steel testing procedures in ASME Sec. III, Div. 5 HBB-2800 [1]. This procedure was designed to assess whether individual material heats possess adequate CF properties and to screen for insufficient long-term creep ductility in materials [16]. Each heat must surpass 200 cycles prior to failure. The mandated test parameters are 595°C a using full reversed strain of ±0.5%, a strain rate of 0.001/s, and a 1-hour tensile hold.

3. RESULTS

3.1. Microstructure Analysis

Optical micrographs are shown in Figure 8 at two different magnifications. Backscatter electron images are shown in Figure 9. For both billets, there was a nonuniform grain-size distribution; however, Billet B, which was HIPed at a higher temperature, has a larger grain size. A more-quantitative grain-size analysis was achieved using EBSD. EBSD images with the inverse-pole-figure (IPF) image overlaid on the image quality (IQ) map is shown in Figure 10. Grain size was determined by fitting an ellipse to each grain distinguished via a high-angle grain boundary (misorientation of 15 degrees) at half of the magnification and same working distance as those shown in Figure 10—i.e., twice the area analyzed. However, this analysis has no statistical significance as it was only performed on one EBSD scan. Bar graphs showing the computed grain-size distributions are shown in Figure 11.

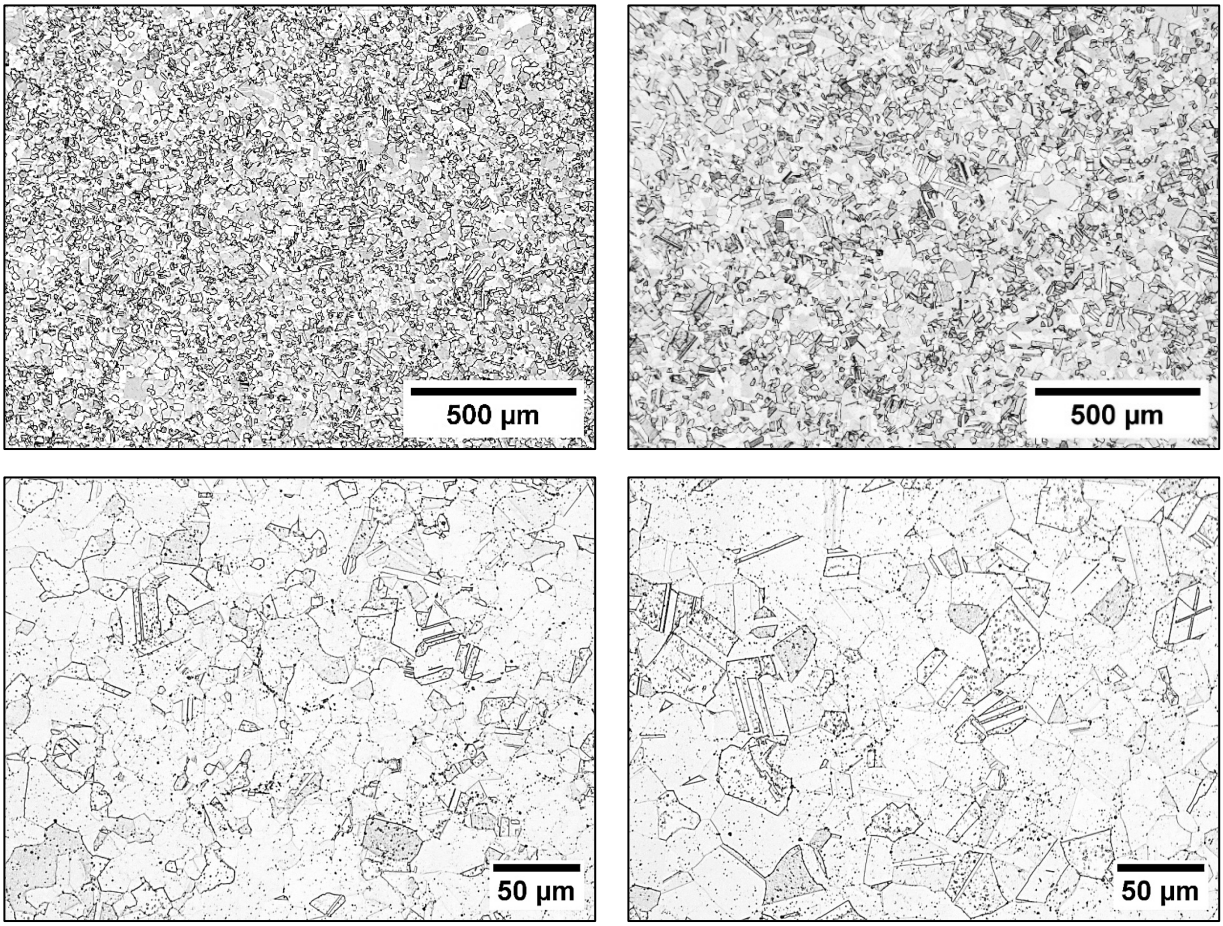

Figure 8. Optical micrographs of PM-HIP 316H stainless steel Billets A (left) and B (right) in the HIP and solution heat-treated (as-received) condition.

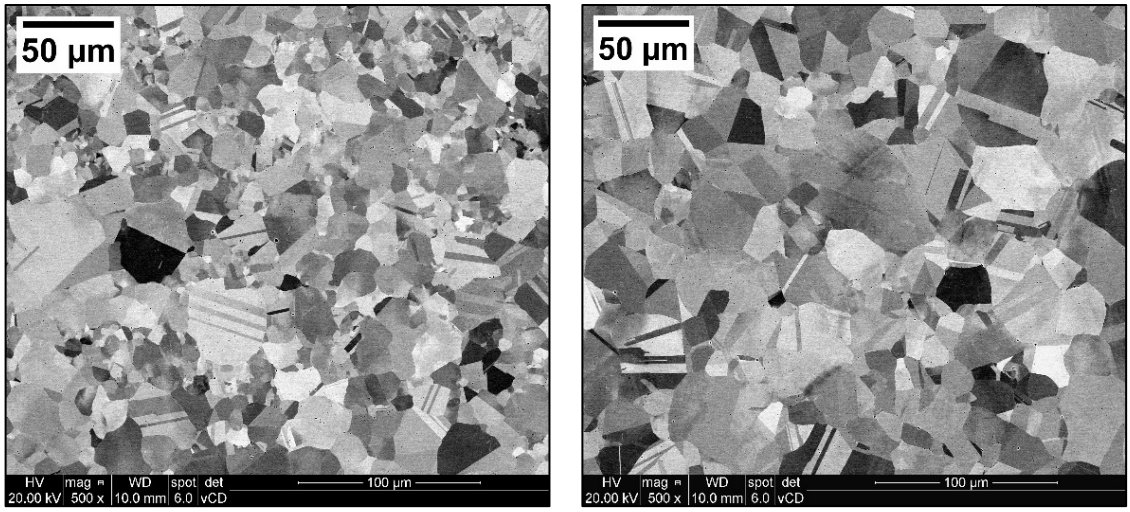

Figure 9. Backscattered electron images of PM-HIP 316H stainless steel Billets A (left) and B (right) in the HIP and solution heat-treated (as-received) condition.

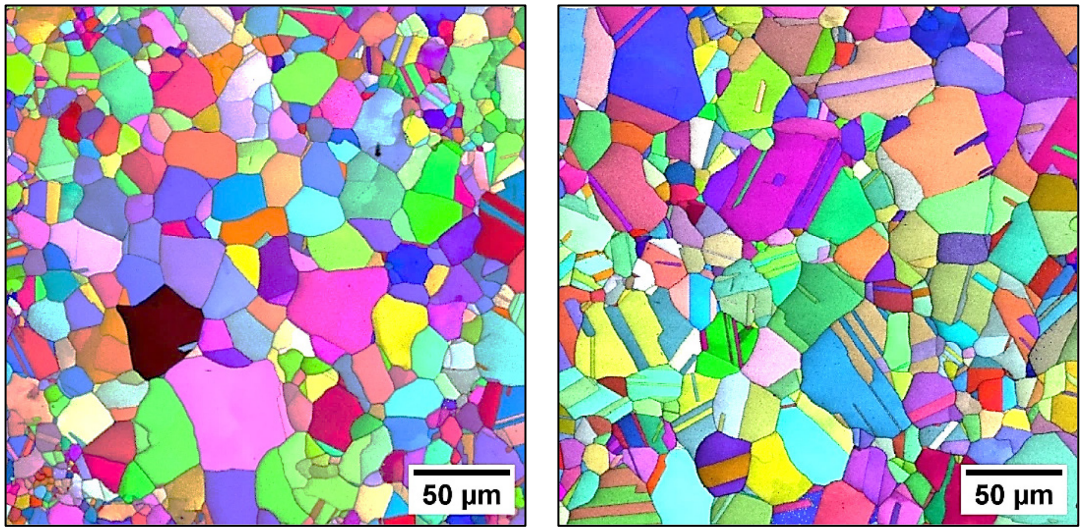

Figure 10. EBSD images showing the IPF map overlayed with the IQ map for PM-HIP 316H stainless steel Billets A (left) and B (right).

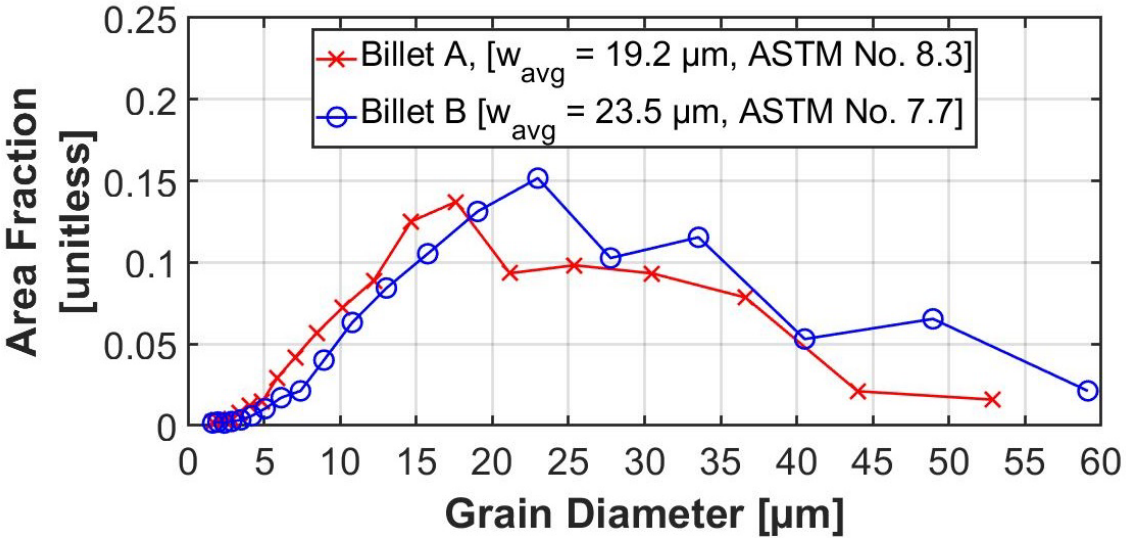

Figure 11. Grain-size distribution plots for PM-HIP 316H stainless steel Billets A and B.

The grain-size distribution for Billet B was shifted to a slightly larger grain size than Billet A, and both billets contained a nonuniform grain size and a nearly bimodal distribution. Because the grains are not entirely uniform nor equiaxed, ASTM E112 [11] is not relevant; therefore, the ellipsoidal fit was chosen.

Higher-magnification backscatter electron images in Figure 12 show particles that are along grain boundaries and within grain interiors. These particle diameters are mostly on the order of 0.5 µm or smaller. Based on qualitative EDS analysis, it is believed that these particles are oxides, typically enriched in Cr, Mn, and/or Mo and depleted of Fe and Ni. Figure 13 shows a secondary-electron image of particles and the corresponding line scan across the particle. These particles are inherent to the powder-based process and remain within the material due to the thermodynamic stability of oxides in 316H stainless steel.

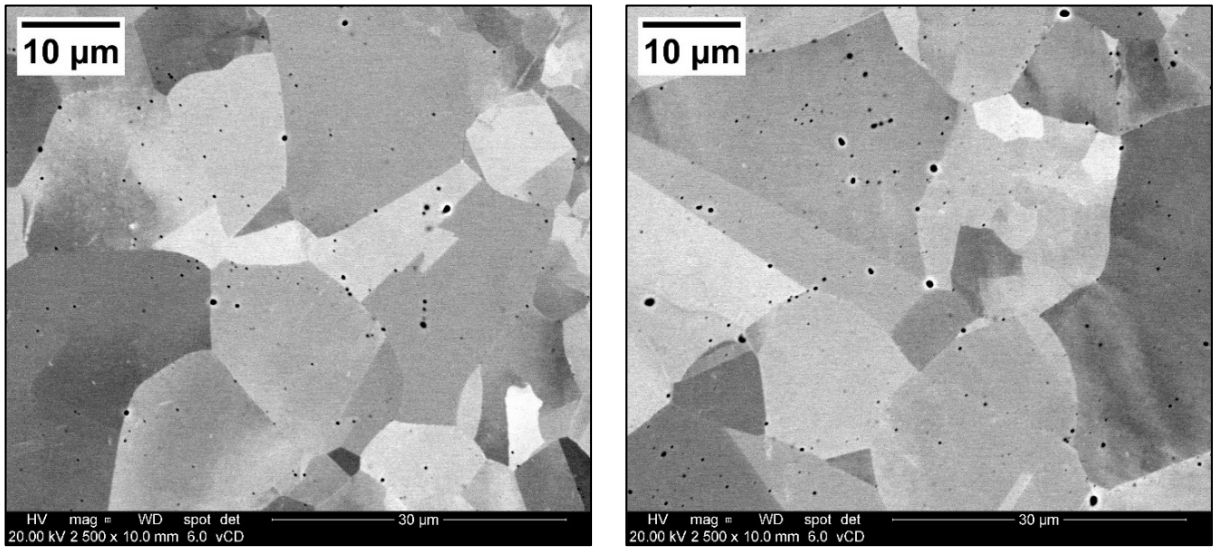

Figure 12. Backscatter electron images of PM-HIP 316H stainless steel Billets A (left) and B (right) in solution heat-treated (as-received) condition.

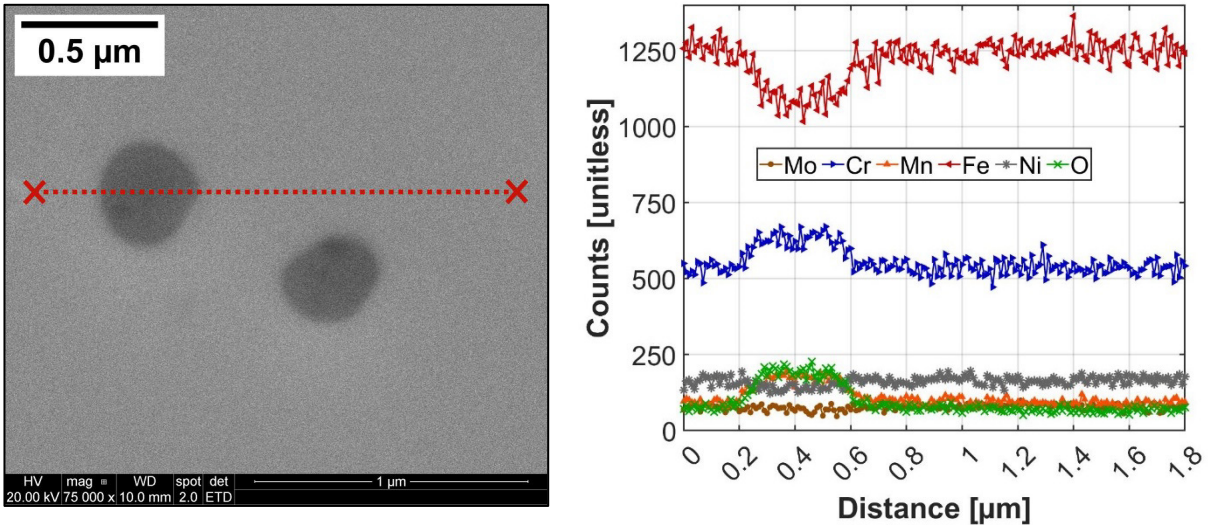

Figure 13. EDS line-scan location across a particle within Billet A (left) and x-ray counts versus position for Cr, Fe, Mn, Mo, Ni, and O (right).

3.2. Mechanical Testing Results

3.2.1. Elevated-Temperature Cyclic Testing

The LCF tests at 650°C for both billets are shown in Figure 14. To visually compare the PM-HIP material with wrought 316H stainless steel, data from Rupp [8] were used. Billet A, with the slightly smaller grain size, showed nearly 300 more cycles prior to failure than Billet B. Both PM-HIP 316H conditions showed fewer cycles to failure than the wrought product, based on the average from two tests. However, the Billet A condition outperformed one of the wrought-material tests. The comparable CF tests are shown in Figure 15. The CF performance maintained a nearly 4× reduction in CF lifetime relative to a wrought material [17]. Failure lifetimes for these materials and the materials tested in prior years shows that little has changed with a reduction in overall oxygen concentration and/or increased HIP temperature. Results for determining whether the material can pass the Sec. III, Div. 5, Clause HBB-2800, [1] fatigue acceptance-test criteria are shown in Figure 16.

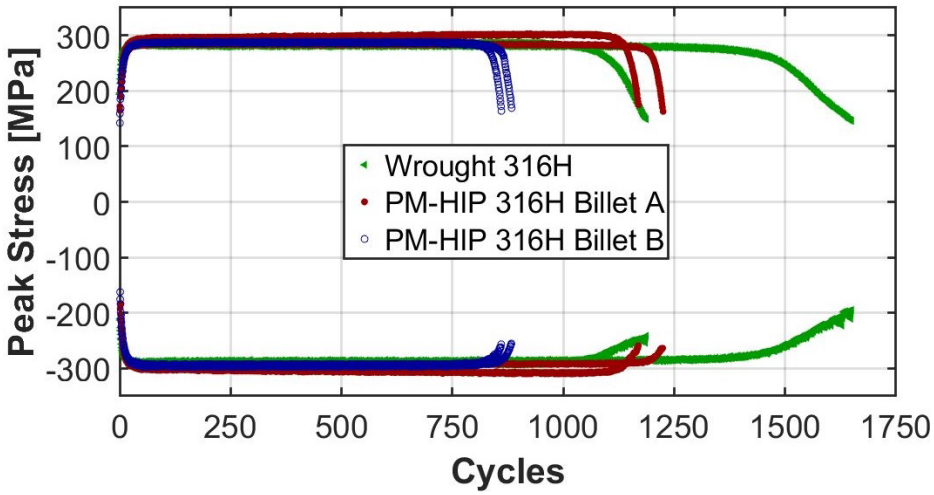

Figure 14. LCF peak stress versus cycles for PM-HIP 316H Billets A and B compared to wrought 316H. Testing was performed at 650°C, ±0.5% strain, and a 0.001/s strain rate.

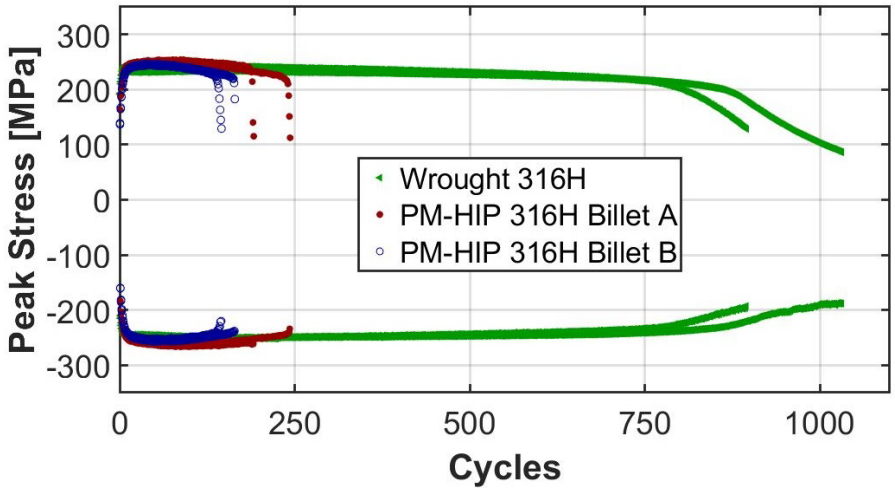

Figure 15. CF peak stress versus cycles for PM-HIP 316H Billets A and B compared to wrought 316H. Testing was performed at 650°C using a ±0.5% strain, a 0.001/s strain rate, and a 30-minute tensile hold.

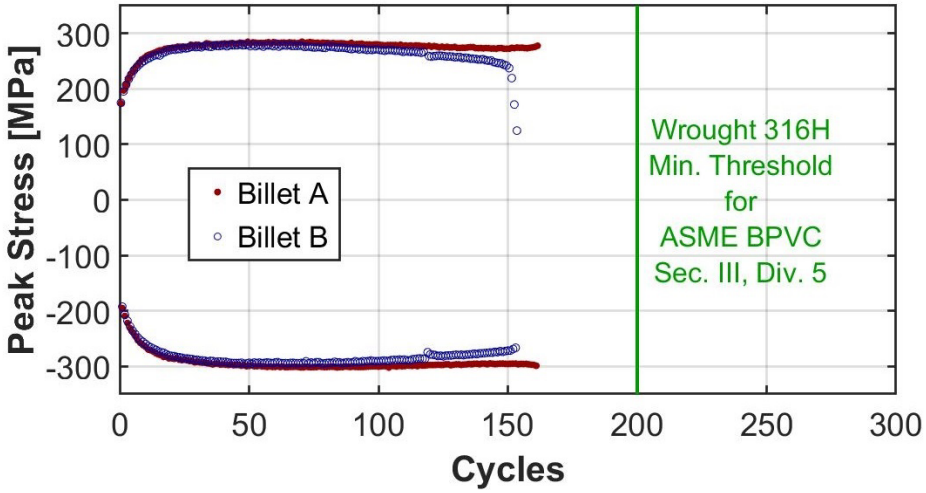

Figure 16. CF peak stress versus cycles for PM-HIP 316H Billets A and B. Testing was performed at 595°C using a ±0.5% strain, a 0.001/s strain rate, and a 1-hour tensile hold according to Sec. III, Div. 5, Clause HBB-2800 [1].

3.2.2. Microstructural Analysis after Cyclic Testing

Figure 17 shows optical micrographs of the crack after LCF testing of Billet A at 650°C. The crack propagation is mostly transgranular, with negligible void nucleation ahead of the main crack. During CF testing, voids nucleated intergranularly and ahead of the main crack, as shown in Figure 18. The same crack-nucleation mechanism occurred with the lower-temperature, longer-hold-time ASME BPVC, Sec. III, Div. 5, CF acceptance tests, as shown with Billet B in Figure 19.

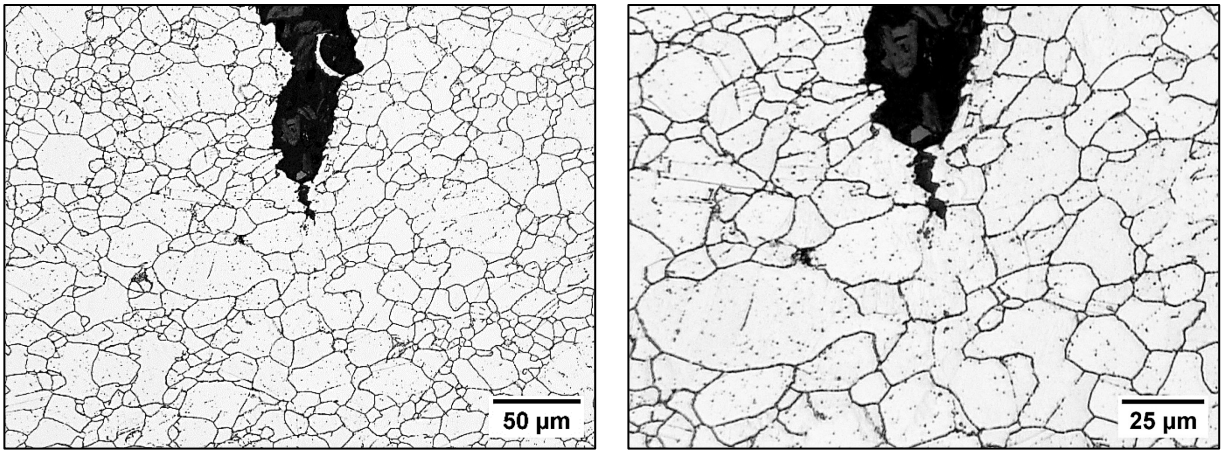

Figure 17. Optical micrographs of Billet A after LCF testing.

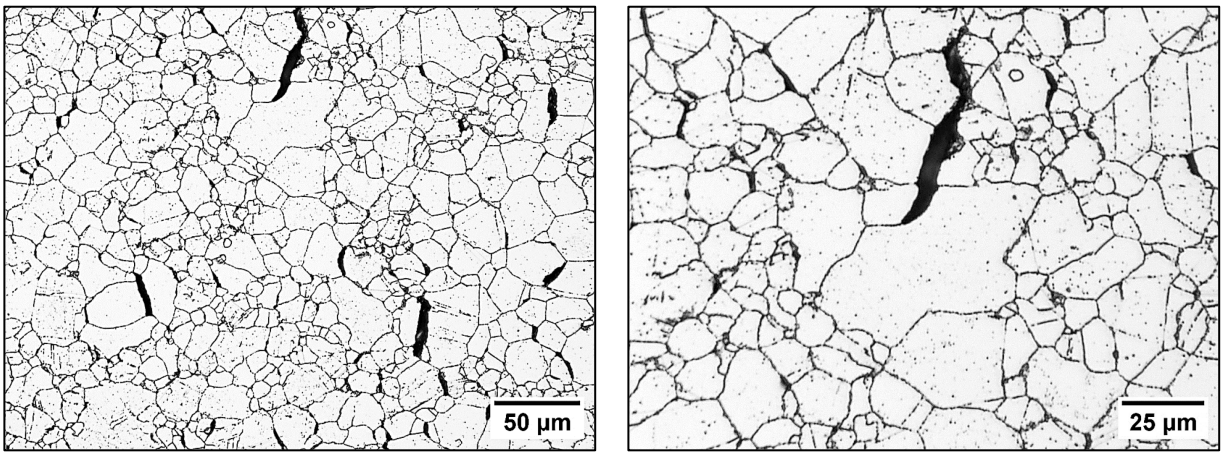

Figure 18. Optical micrographs of Billet A after CF testing at 650°C with a 30-minute tensile hold.

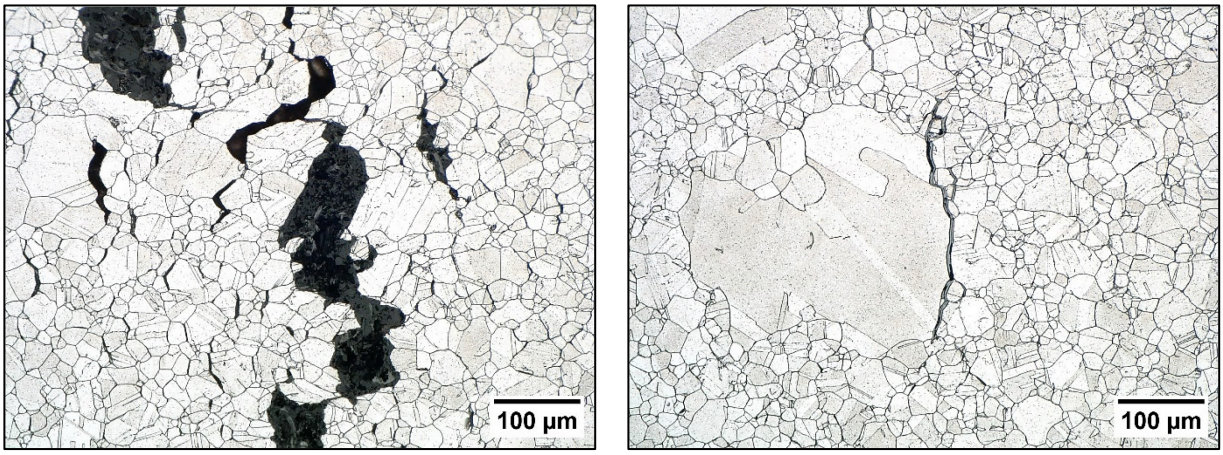

Figure 19. Optical micrographs showing cracks in the PM-HIP 316H Billet B material tested at 595°C and a 1-hour tensile hold according to the ASME BPVC Sec. III, Div. 5, [1] acceptance-test criteria.

3.3. Grain Growth Investigation

The purpose of this investigation is to explore the feasibility of achieving a grain size of ASTM No. 7 or coarser for PM-HIP 316H and to determine whether the precipitates at the grain boundaries can be reduced or dissolved. Optical micrographs of Billet A and B after the 1200°C heat-treatment are shown in Figure 20, and EBSD images are shown in Figure 21. Both billets showed large grain growth at 1200°C for 1 hour, with the grain size, increasing beyond that of the original powder diameter. Although much-larger grains exist, small grains remained, and the larger grains contained internal twins with a high degree of misorientation. The effect of bimodal grain size distribution on the cyclic performance requires further experimental evaluation.

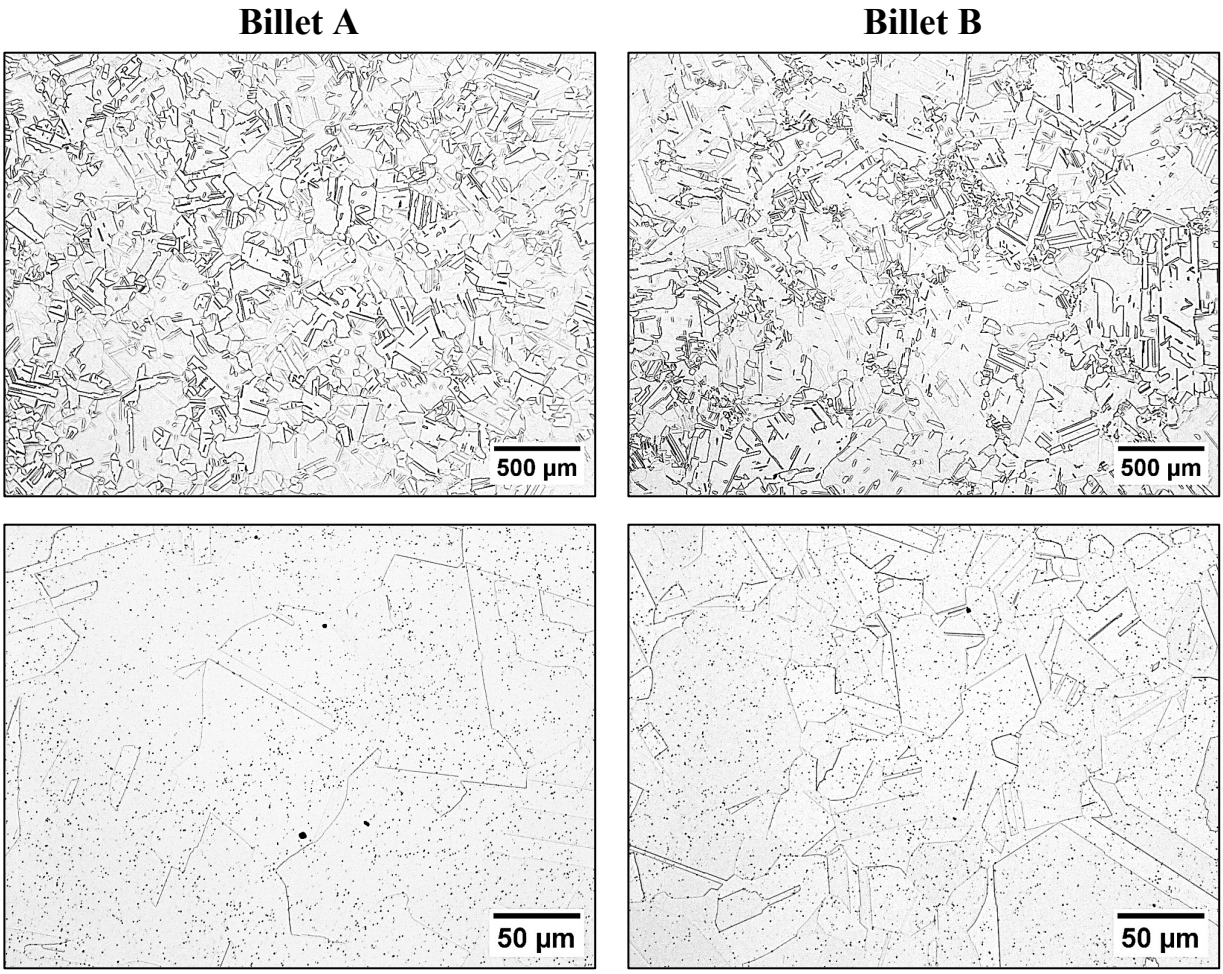

Figure 20. Optical micrographs of Billets A (left) and B (right) after a 1-hour heat treatment at 1200°C.

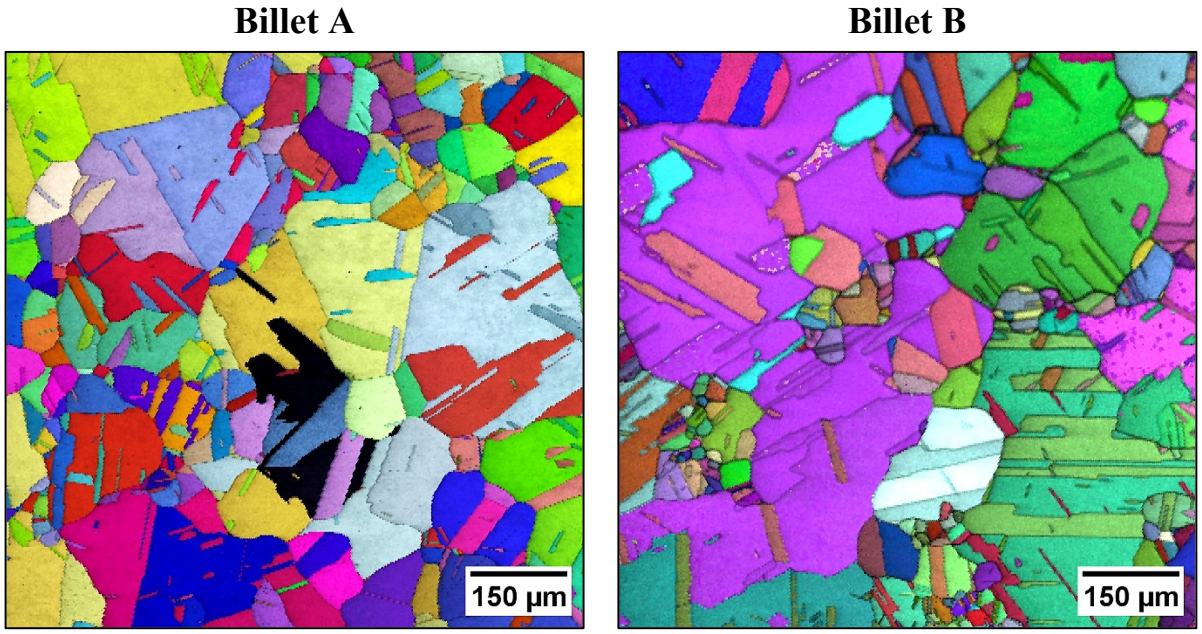

Figure 21. EBSD images of Billets A (left) and B (right) after a 1-hour heat treatment at 1200°C showing EBSD IPF/IQ images.

4. SUMMARY

The powder chemistries and HIP parameters analyzed in this work did not indicate an improvement in CF performance compared to previous 316 stainless steel chemistries analyzed. Specifically, the lower oxygen concentration did not result in changes to PM-HIP 316 stainless steel performance. Although, both Billets showed much lower CF resistance than wrought, the slightly larger grain size in Billet B, as compared to Billet A, did not improve CF performance. It is likely that the other microstructural differences are the primary factor resulting in reduced CF. An additional laboratory-scale heat treatment showed the ability to induce grain growth at 1200°C for one hour. However, the grains resulted in a bimodal size distribution, which will require further experimental evaluation for understanding the cyclic performance.

5. FUTURE WORK

Because the main failure mechanism seems to be associated with creep damage during the CF test, future work must specifically analyze the creep behavior of PM-HIP 316H stainless steel. This would determine whether CF performance is a combinatory influence of creep and fatigue, or solely related to reduced creep performance associated with PM-HIP 316 stainless steels. The only known data that showed creep performance of PM-HIP 316 stainless steel is from Östlund and T. Berglund [18], which showed similar creep rupture times as wrought 316 stainless steel. In addition, other materials should be analyzed for their ability to be processed via PM-HIP for comparison to their wrought-material counterparts.

6. REFERENCES

[1] ASME International. 2023. "Division 5 High Temperature Reactors," in *Section III Rules for Construction of Nuclear Facility Components* ed, 2023.

[2] Callaghan, M., M. Chatterton, D. Coon, and A. Wisbey. 2020. “High Temperature Mechanical Performance of Type 316L Austenitic Stainless Steels Manufactured by the Powder Metallurgy

Hot Isostatic Pressing Process." in *Pressure Vessels and Piping Conference PVP2020*, 2020: ASME.
[3] Kyffin, W., D. Gandy, and B. Burdett. 2020. "A Study of the Reproducibility and Diversity of the Supply Chain in Manufacturing Hot Isostatically Pressed Type 316L Stainless Steel Components for the Civil Nuclear Sector." *ASME Journal of Nuclear Radiation Science* 6(2): 021116. https://doi.org/10.1115/1.4044752.
[4] Cooper, A. J., N. I. Cooper, J. Dhers, and A. H. Sherry. 2016. "Effect of Oxygen Content Upon the Microstructural and Mechanical Properties of Type 316L Austenitic Stainless Steel Manufactured by Hot Isostatic Pressing" *Metallurgical and Materials Transactions A* 47(9): 4467–4475. https://doi.org/10.1007/s11661-016-3612-6.
[5] ASME International, "Case N-834 ASTM A988/A988M-11 UNS S31603, Subsection NB, Class 1 Components Section III, Division 1," ed, 2013.
[6] ASME International, "Section III Rules for Construction of Nuclear Facility Components," in *Division 1 — Subsection NB Class 1 Components*, ed: ASME International, 2023.
[7] Rupp, R., and R. Wright. 2020. "The Elevated-Temperature Cyclic Properties of Alloy 316L Manufactured using Powder Metallurgy Hot Isostatic Pressing." INL/EXT-20-59327, Idaho National Laboratory, Idaho Falls, ID. https://gain.inl.gov/content/uploads/4/2024/04/Document-INL-EXT-20-59327.pdf.
[8] Rupp, R. 2021. "The Elevated-Temperature Cyclic Properties of Alloy 316H Fabricated by Powder Metallurgy Hot Isostatic Pressing." INL/EXT-21-62993, Idaho National Laboratory, Idaho Falls, ID. https://doi.org/10.2172/1975813.
[9] ASME International, 2023. "Part A: Ferrous Material Specifications." in *BPVC Section II Materials*.
[10] ASTM International, 2023. "Standard Specification for Hot Isostatically-Pressed Stainless Steel Flanges, Fittings, Valves, and Parts for High Temperature Service." A988/A988M-17, Last updated May 22.
[11] ASTM International. 2024. " Standard Test Methods for Determining Average Grain Size." E112-24, Last updated June 28.
[12] ASTM International. 2021. " Standard Test Method for Strain-Controlled Fatigue Testing." E606/E606M-21, Last updated July 2.
[13] ASTM International. 2020. "Standard Test Method for Creep-Fatigue Testing." E2714-13(2020), Last updated May 6.
[14] Idaho National Laboratory. 2017. "Creep Fatigue Testing." PLN-3346, Idaho National Laboratory, Idaho Falls, ID.
[15] Totemeier, T. and H. Tian. 2007. "Creep-fatigue–environment Interactions in INCONEL 617." *Materials Science and Engineering: A* 468–470: 81–87. https://doi.org/10.1016/j.msea.2006.10.170.
[16] Jetter, R., Mitchell, M., and Morton, D., "Division 5—High Temperature Reactors." Online Companion Guide to the ASME Boiler & Pressure Vessel Codes," ed: ASME Press, 2020.
[17] Patterson, T., and T. -L. Sham. 2023. "An Initial Evaluation of the Elevated-Temperature Cyclic Properties of Optimized 316H Stainless Steel Fabricated by Powder Metallurgy Hot Isostatic Pressing." INL/RPT-23-75644, Idaho National Laboratory, Idaho Falls, ID. https://www.osti.gov/servlets/purl/2222878.
[18] Östlund, M., and T. Berglund. 2019. "Overview of properties, features and developments of PM HIP 316L and 316LN." in *Hot Isostatic Pressing HIP'17*, edited by Pranesh Dayal and Gerry Triana, Materials Research Forum LLC, Millersville, PA. https://dx.doi.org/10.21741/9781644900031-17.